Formation of metallic colloids in CaF$_2$ by intense ultraviolet light

Stephan Rix,[1,2,a] Ute Natura,[3] Felix Loske,[4,5] Martin Letz,[1] Claudia Felser,[2] and Michael Reichling[4]

[1]Schott AG, Hattenbergstr. 10, 55122 Mainz, Germany
[2]Institut für Anorganische und Analytische Chemie, Johannes Gutenberg-Universität, Staudingerweg 9, 55099 Mainz, Germany
[3]Hellma Materials GmbH & Co. KG, Moritz-von-Laue-Str. 1, 07745 Jena, Germany
[4]Fachbereich Physik, Universität Osnabrück, Barbarastr. 7, 49076 Osnabrück, Germany
[5]Institut für Physikalische Chemie, Johannes Gutenberg-Universität, Jakob-Welder-Weg 11, 55099 Mainz, Germany

Highest purity CaF$_2$ single crystals are irreversibly modified when irradiated with millions of pulses of 193 nm light at fluences of 120 mJ/cm^2. Mie theory explains the observed haze by attributing the wavelength dependent extinction and the ratio between absorption and scattering to metallic colloids with radii in the range of 20 to 30 nm and a fractional volume of up to $2.8 \cdot 10^{-7}$. Non-contact scanning force microscopy (NC-AFM) measurements performed on a surface produced by *in-vacuo* cleavage reveals that laser irradiation additionally produces a 10^4 times higher volume density of colloids with a radius of 1 to 2 nm. © 2011 American Institute of Physics. [doi:10.1063/1.3673301]

For the foreseeable future, deep ultraviolet (DUV) microlithography will be performed with 193 nm radiation (ArF excimer laser),[1] involving lenses and windows exposed to different light intensities. While fused silica is used in areas of low radiation density,[2] single crystalline CaF$_2$ is the material of choice in areas of high radiation density due to its laser durability, chemical resistance, and suitable mechanical properties.[1,3] Since it has a cubic structure, CaF$_2$ exhibits only minute birefringence[4,5] and allows the construction of large optical elements.

However, subjected to extreme radiation doses, intrinsic[6] and extrinsic[7] defects facilitate laser damage in CaF$_2$ optical components, showing as haze and extinction at visible and UV wavelengths. The nature of such damage is subject of ongoing research and Ca colloids have been suggested as its origin.[8,9] CaF$_2$ is susceptible to colloid formation as the Ca sub-lattice differs only slightly in the lattice constant from metallic Ca. Therefore, colloids can be formed by removing fluoride atoms from lattice sites to remote interstitial sites, which has been studied in the bulk[10,11] and at the surface[12,13] of electron-irradiated CaF$_2$.

Here, we investigate Ca colloid formation in CaF$_2$ upon 193 nm laser light irradiation and characterize colloids by optical spectroscopy and dynamic scanning force microscopy operated in the non-contact mode (NC-AFM).

We observe haze in CaF$_2$ samples of 38 mm diameter and $4 - 6$ mm thickness after use as a laser window in a 193 nm excimer laser (LPX 220i, Coherent GmbH, Göttingen, Germany). Samples of different laser durability classes, denoted as W1 with the highest to W4 with the lowest durability, are investigated. The samples' transmission is measured in the spectral range of $200 - 800$ nm in a spectrometer (Specord 250, Analytik Jena AG, Jena, Germany) before and after irradiation with up to $2 \cdot 10^8$ pulses with a pulse duration of $25 - 30$ ns, an average fluence of 120 mJ/cm^2 and

repetition rates of $60 - 100$ Hz. The laser beam has a top hat spatial beam profile of dimensions 5 mm $\times$ 20 mm.

For NC-AFM measurements, the samples are cleaved[14] and transferred to the force microscope in an ultra-high vacuum system maintaining a base pressure of 1×10^{-10} mbar. Measurements are performed with a commercial microscope (VT-AFM 750, RHK, Troy, MI, USA) and commercial probes (type FM, Nanoworld, Neuchtel, Switzerland) which are sputter cleaned prior to use. The cantilever is excited to oscillation at its resonance frequency (70 kHz) with an amplitude of 20 nm. The detuning Δf of the cantilever resonance frequency is measured by a phase locked loop detector. Images are acquired in the topography mode, where the detuning is kept constant by a regulation loop acting on the piezo element controlling the tip-surface distance. The error signal from the loop directly reflects the topographic contrast z. The finite time constant of the loop results in a residual detuning contrast when the tip-surface interaction changes rapidly.[15] For an easy detection of surface irregularities, we display the residual Δf signal. Such images do not allow a detailed topographic analysis, however, it is straightforward to identify an irregularity as a surface pit or protrusion by relating the change from dark to bright contrast or vice versa to the scanning direction. An average electrostatic force resulting from surface charges is measured and compensated as described elsewhere.[16]

Scattering and absorbing defects generated by laser irradiation result in a characteristic wavelength dependent extinction (Fig. 1),[17] which we attribute to Ca colloids in the crystal. The extinction peak at 375 nm also shows the presence of F-centers.[18] The samples exhibit a clear correlation of defect generation with their laser durability classification. However, samples with similar extinction may have different absorption and scattering characteristics in the visible range, as evident from optical transmission and dark field images (Fig. 2).

Sample W3 shows small absorption and strong scattering, while sample W4 exhibits the opposite behavior.
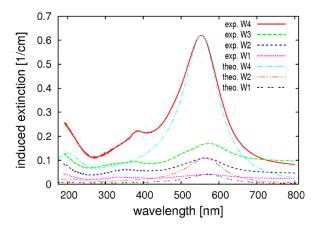
a)Electronic mail: rixs@uni-mainz.de.

FIG. 1. (Color online) Measured spectral extinction of CaF$_2$ laser windows induced by 193 nm light irradiation (see Ref. 17). The induced extinction decreases with increasing laser durability from sample W4 to W1. The extinction is attributed to metallic colloids, whose predominant radii are determined to be 22 (W4), 26 (W2), and 28 (W1) nm by a fit of Mie theory cross sections (theo.) to experimental data (exp.).
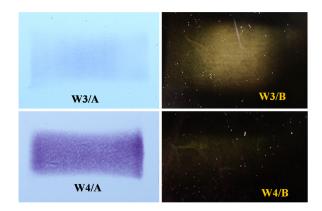

FIG. 2. (Color online) Absorption (A) and scattering (B) in windows W3 and W4 after 193 nm light irradiation as observed by optical transmission and dark field imaging (see Ref. 17).

Surprisingly, the extinction curves for samples W3 and W4 in Fig. 1 are qualitatively similar, pointing to complementary contributions of absorption and scattering to the overall extinction.

For a better understanding, we calculate the absorption, total scattering, and extinction cross sections for Ca colloids in CaF$_2$ from Mie-theory,[19] considering corrections of the refractive index of Ca due to the colloid size.[20] We only consider single scattering as the scatterers are very dilute. The spectra for monodisperse colloids are calculated for radii of 1, 10, 22, 50, and 100 nm with a colloid fractional volume $\eta = 10^{-6}$ (Fig. 3), where η describes the fraction of CaF$_2$ converted into Ca.

The results demonstrate a significant dependence of the absorption and scattering contributions on the colloid size, namely extinction is clearly dominated by absorption for small colloids while scattering is important for large colloids. This is explained by the fact that the electromagnetic wave only penetrates into a thin shell of the metallic colloid with a thickness of the order of $(nc\epsilon_0)/\sigma$, where n is the real part of the refractive index, c is the speed of light, ϵ_0 is the vacuum permittivity, and σ is the conductivity.

In a fit to experimental data (Fig. 1), the peak position is matched by adjusting the colloid radius while the peak height is adjusted to determine the colloid fractional volume. For samples W1, W2, and W4, we determine colloid radii of 28, 26, and 22 nm and colloid fractional volumes of 2.0×10^{-8}, 5.1×10^{-8}, and 2.8×10^{-7}, respectively, converting to a colloid volume density between 10^{-4} and $10^{-3} \mu m^{-3}$. However, colloids are not monodisperse, but a certain distribution of colloid sizes is evident from the fit curves (Fig. 1) which all have significantly narrower peaks than the experimental spectra. Comparing experimental data (Figs. 1 and 2) and model predictions (Fig. 3), we conclude that sample W4 contains a large fraction of small colloids while sample W3 contains a large fraction of large colloids.

The presence of small Ca colloids is confirmed by NC-AFM measurements on sample W4 (Fig. 4). In addition to expected features of cleaved non-irradiated CaF$_2$,[14] a zero surface potential[16] is found, pointing to an enhanced conductivity of the irradiated sample due to the colloids. The characteristic features observed for sample W4 are randomly distributed shallow pits and small protrusions (Fig. 4(a)). We interpret protrusions as remainders of colloids and pits as cavities left by colloids removed in the cleavage process. Analyzing several non-overlapping images, we find a similar number of pits (59) and protrusions (55), resulting in an areal
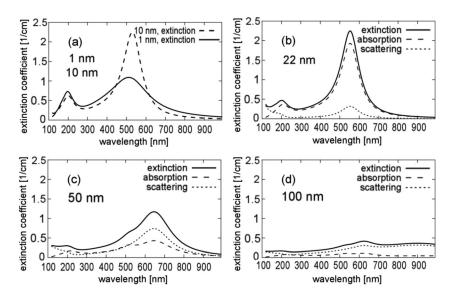

FIG. 3. Extinction, absorption and total scattering cross sections from Mie theory calculations for 1, 10, 22, 50, and 100 nm colloids assuming a colloid fractional volume of 10^{-6}. The total extinction decreases with increasing colloid size, however, the ratio of scattering to absorption increases strongly. For colloids with radii below 10 nm scattering is negligible.
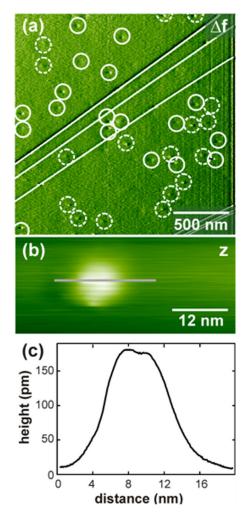
FIG. 4. (Color online) NC-AFM images of a cleavage face of sample W4. (a) Overview image exhibiting 17 pits (colloid cavities, solid circles) and 18 protrusions (colloid remainders, dashed circles). The residual Δf signal shows surface irregularities as split features with a bright/dark contrast. With horizontal scan lines and the fast scan direction from left to right, irregularities can be identified as pits or protrusions according to the bright contrast being on the right or left side. (b) Magnified view of a protrusion with the topography signal displayed. (c) Cross-section through the protrusion taken along the horizontal line shown in frame (b).

fractional volume of 1.4×10^{-7} matching the colloid fractional volume of the large colloids.

We conclude that upon irradiation with 193 nm laser light, under conditions typically experienced by optical materials in high power UV lasers, a volume fraction of the order of 10^{-7} of CaF_2 is converted into Ca colloids. We observe large colloids with radii of $20 - 30$ nm, similar to sub-surface colloids generated by energetic electrons,[13] and small colloids with radii of $1 - 2$ nm, in a composition probably resulting from processes of defect generation,[6] agglomeration,[21] ripening,[11] and laser induced bleaching[8] competing during irradiation and dark times. We find that colloid formation depends on the laser durability of CaF_2 and highest quality CaF_2 has the lowest void generation rate with the formed colloids presumably having a broad size distribution as ripening is slow due to the low density of colloids. Further knowledge about this distribution can be helpful for efforts of curing laser induced haze by optical excitation of the colloids. Our experiments do not allow a prediction for a formation rate of colloids, however, a theoretical estimate has been made elsewhere.[22]

colloid density of $5\,\mu m^{-2}$. For an average protrusion, we yield a radius of 4 nm and a height of 180 pm from its topography (Fig. 4(b)) and cross section (Fig. 4(c)), resulting in an estimated colloid radius of $1 - 2$ mm. To estimate the colloid volume density from the areal density, we assume a statistical distribution of colloids on a square lattice with a lattice constant of 325 nm that is of the order of the actual average nearest neighbor distance of 240 nm. It is straightforward to construct a three-dimensional lattice yielding a colloid volume density of $15\,\mu m^{-3}$, which converts to a colloid

[1]M. Rothschild, Mater. Today **8**, 18 (2005).
[2]U. Natura, O. Sohr, R. Martin, M. Kahlke, and G. Fasold, Proc. SPIE **5273**, 155 (2004).
[3]P. Maushake, Opt. Photon. **2**, 46 (2008).
[4]J. H. Burnett, Z. H. Levine, and E. L. Shirley, Phys. Rev. B **64**, 241102 (2001).
[5]M. Letz, L. Parthier, A. Gottwald, and M. Richter, Phys. Rev. B **67**, 233101 (2003).
[6]R. Lindner, M. Reichling, R. T. Williams, and E. Matthias, J. Phys. Condens. Matter. **13**, 2339 (2001).
[7]J. Sils, S. Hausfeld, W. Clauß, U. Pahl, R. Lindner, and M. Reichling, J. Appl. Phys. **106**, 063109 (2009).
[8]L. P. Cramer, S. C. Langford, and J. T. Dickinson, J. Appl. Phys. **99**, 054305 (2006).
[9]X. Hu, Y. Dai, L. Y. Yang, J. Song, C. S. Zhu, and J. R. Qiu, J. Appl. Phys. **101**, 023112 (2007).
[10]L. T. Chadderton, E. Johnson, and T. Wohlenberg, Radiat. Eff. Defects Solids. **28**, 111 (1976).
[11]E. A. Kotomin, V. N. Kuzovkov, and A. I. Popov, Radiat. Eff. Defects Solids **155**, 113 (2001).
[12]M. Reichling, R. M. Wilson, R. Bennewitz, R. T. Williams, S. Gogoll, E. Stenzel, and E. Matthias, Surf. Sci. **366**, 531 (1996).
[13]R. Bennewitz, D. Smith, and M. Reichling, Phys. Rev. B **59**, 8237 (1999).
[14]L. Tröger, J. Schütte, F. Ostendorf, A. Kühnle, and M. Reichling, Rev. Sci. Instrum. **80**, 063703 (2009).
[15]S. Gritschneder, Y. Namai, Y. Iwasawa, and M. Reichling, Nanotechnology **16**, S41 (2005).
[16]S. Gritschneder and M. Reichling, Nanotechnology **18**, 044024 (2007).
[17]U. Natura, S. Rix, M. Letz, and L. Parthier, Proc. SPIE **7504**, 75041P (2009).
[18]Y. Ma and M. Rohlfing, Phys. Rev. B **77**, 115118 (2008).
[19]G. Mie, Ann. Phys. **330**, 377 (1908).
[20]V. M. Orera and E. Alcalá, Phys. Status Solidi **44**, 717 (1977).
[21]M. Letz and L. Parthier, Phys. Rev. B **74**, 064116 (2006).
[22]S. Rix, Ph.D. thesis, Johannes Gutenberg-Universität, 2011.